The persistence of viscous effects in the overlap region, and the mean velocity in turbulent pipe and channel flows

Katepalli R. Sreenivasan and Anupam Sahay
Mason Laboratory, Yale University
New Haven, CT 06520-8286

Abstract

We expand on our previous argument (Sreenivasan 1987) that important elements of the dynamics of wall-bounded flows reside at the wall-normal position y_p corresponding to the peak of the Reynolds shear stress. Specializing to pipe and channel flows, we show that the mean momentum balance in the neighborhood of y_p is distinct in character from those in the classical inner and outer layers. We revisit empirical data to confirm that $y_p = O((h\nu/U_*)^{1/2})$ and show that, in a neighborhood of order $R_*^{1/2}$ around y_p, only the viscous effects balance pressure-gradient terms. Here, $R_* = hU_*/\nu$, h is the pipe radius or channel half-width, ν is the kinematic viscosity of the fluid and U_* is the friction velocity. This observation provides a mechanism by which viscous effects play an important role in regions traditionally thought to be inviscid or inertial; in particular, it throws doubt on the validity of the classical matching principle. Even so, it is shown that the classical semi-logarithmic behavior for the mean velocity distribution can be a valid approximation. It is argued that the recently advanced power-law profiles possess a rich underlying structure, and could be good approximations to the data over an extended region (but they too are unlikely to be exact).

1 Introduction

Essentially all the important notions in wall-bounded flows are cast in terms of two length scales: the inner or viscous scale ν/U_*, where ν is the kinematic viscosity of the fluid and U_* is the friction velocity ($\equiv \sqrt{\tau_w/\rho}$, τ_w and ρ being the wall shear stress and fluid density, respectively), and the outer scale h, where h is the pipe radius, channel half-width or boundary layer thickness. The ratio of the two scales is the Reynolds number $R_* = hU_*/\nu$. Since the appropriate asymptotics correspond to the limit $R_* \to \infty$, one may expect that the problem has elements of singular perturbation. We shall use the standard notation that $U^+ = U/U_*$ and $y^+ = yU_*/\nu$, y being the normal distance from the wall. It is traditionally thought that the viscous effects are important up to a y^+ of about 30 and that, within this region, the outer length scale h is unimportant. In the bulk of the flow excluding this viscous region, it is thought that ν is unimportant and the characteristic length is h. This view has been quite successful in organizing various experimental data (see, e.g., Sreenivasan 1989,

Dussauge *et al.* 1996), though it has been recognized for some time (e.g., Rao *et al.* 1971) that the interaction between the two scales is the key to the flow structure.

In an earlier paper (Sreenivasan 1987), we noted that a proper understanding of the boundary layer structure requires greater emphasis on wall-normal position where the Reynolds shear stress peaks. This peak position scales as the geometric mean of the inner and outer length scales. It is well known (e.g., Drazin & Reid 1981) that, in linear and early stages of nonlinear instability in boundary layers and channel flows, the position of the peak Reynolds shear stress coincides with the critical layer. This observation was inverted in Sreenivasan (1987) to suggest that the position of the peak Reynolds shear stress, y_p, in turbulent wall flows plays something of the same role as that of the critical layer in unstable wall flows. It was pointed out that, just as for critical layer in unstable wall flows, the mean velocity at y_p is approximately a constant fraction of the freestream or centerline velocity, the fraction being about 0.65. Other analogies between the critical layer in the unstable state and the 'critical layer' in the turbulent state were also cited.

The critical layer in unstable boundary layers is the seat of perturbation vorticity which undergoes amplification when the Reynolds number exceeds a certain threshold. The next stages of the perturbation development involve the onset of three dimensionalities and, eventually, of turbulence itself. If the turbulent vorticity in the boundary layer can be caricaturized as a vortex sheet, it was thought by analogy that its seat would be y_p. By interaction with image vorticity (invoked to mimic the presence of the wall), this hypothetical vortex sheet located at y_p gets lumped first into two-dimensional rolls and, eventually, into horse-shoe shaped vortices. These latter structures are comparable in several respects to those found from visualization studies of the boundary layer (e.g., Head & Bandyopadhyay 1981). It was further argued, albeit with less certainty, that the same picture can explain aspects of the structure in the wall region, for example the (noisy) spanwise periodicity of streaks (Kline *et al.* 1967). For quantitative details and comparisons with data, one should consult Sreenivasan (1987).

Whatever the detailed objections to the physical content of the model and however preliminary the attempt, it appeared that a self-contained picture of the boundary layer could be developed on that basis. Unlike in the predecessor paper (Sreenivasan 1987) which focused on the large-scale structural elements of the boundary layer, we shall examine here the mean velocity distribution to reiterate, in quite a different way, the importance of the 'critical layer'. This seems to be an especially timely goal because of the renewed interest and recent controversy surrounding the mean velocity distribution in pipe flows (e.g., Barenblatt & Chorin 1996, Zagarola & Smits 1997).

In the classical picture, one *assumes* the existence of a common region of validity of the outer and inner solutions of $\partial U^+(R_*, y^+)/\partial y^+$ in the limit $R_* \to \infty, y^+ \to \infty$, and puts forth asymptotic arguments to obtain

$$U^+(R_*, y^+) = (1/\kappa) \ln y^+ + B, \tag{1}$$

where κ and B are empirical constants presumed to be independent of R_*. This is the celebrated log-law, which occupies a central place in the turbulence literature (e.g., Coles &

Hirst 1969, Monin & Yaglom 1971, Tennekes & Lumley 1972). It is generally thought that $y^+ \approx 30$ and $y^+ \approx 0.15R_*$ are the lower and upper limits of the logarithmic profile and the Kármán constant $\kappa \approx 0.4$ and $B \approx 5.5$ (see, for example, Coles & Hirst 1969). There is still some uncertainty about these constants: recent high-Reynolds-number measurements in pipe flows (Zagarola 1996) yield $\kappa = 0.44$ and $B = 6.1$.

There exist alternative formulations for the overlap region (Long & Chen 1981, Barenblatt 1993, Barenblatt & Chorin 1996, George *et al.* 1996, George & Castillo 1996). Here, we shall restrict attention to Barenblatt's formulation. Its primary contention is that the limit of small-viscosity (or high Reynolds number) is singular—as is common in second-order phase transitions in condensed matter (Domb & Green 1976) and also, perhaps, in Kolmogorov turbulence (Monin & Yaglom 1975)—and so the viscous effects never disappear in the overlap region. This imperils the classical matching argument and the orthodox view that the log-law is exact in the infinite Reynolds number limit. Specifically, note that dimensional considerations allow us to write the velocity distribution in an intermediate layer in the form

$$y^+(\partial U^+/\partial y^+) = \psi(y^+, R_*), \tag{2}$$

where ψ is an unknown function of its arguments. In the classical picture, ψ is thought to asymptote to a constant, say $1/\kappa$, as the arguments of ψ, namely R_* and y^+, assume large values. Integration then yields the log-law. On the other hand, suppose that

$$y^+(\partial U^+/\partial y^+) = (1/\kappa)(y^+)^\alpha, \tag{3}$$

α being some positive constant. This leads to a power-law for the mean velocity distribution. In particular, Barenblatt (1993) and Barenblatt & Chorin (1996) predict the asymptotic nature of U^+ in two regions of the flow—the classical overlap region (say B1) and a region further out towards the center (say B2). In the power-law paradigm, B1 + B2 together form the overlap region. The specific predictions are the following: (a) In B1, U^+ is tangent to the classical logarithmic profile to which it remains close but from which it always remains distinct. (b) In B2, the power law can be approximated properly by a logarithmic function similar to the classical log-law but with a slope that is approximately $\sqrt{\mathrm{e}}$ times that of the classical value. It may be thought that this latter prediction does not contradict the classical log-law because the domains of the two logarithmic regions are disjoint. However, because B2 would be a part of the outer region in the classical picture, one may consider that a conflict does exist here as well.

The purpose of this paper is to examine the nature of the mean velocity distribution briefly, emphasizing along the way two significant qualitative issues: (a) The viscous effects are important in a region of pipe and channel flows that is traditionally thought to be inviscid and that, in fact, the balance there is between viscous and pressure gradient effects. Following Long & Chen (1981), we might call this 'critical' region a *mesolayer* (although we do not necessarily subscribe to all the implications of that work). The existence of such a mesolayer gives a new twist to the dynamics of the boundary layer, but the degree to which

the classical picture needs modification is not yet clear (see section 4). (b) The importance of viscosity in the mesolayer offers a key to the regeneration mechanism of the boundary layer. The discussion here will be necessarily brief, and more details will be published elsewhere (Sahay & Sreenivasan 1996).

2 The background

2.1 The wall-normal position of the peak of the Reynolds shear stress

Central to the present arguments is the manner in which the Reynolds or turbulent shear stress, $\tau \equiv -\langle uv \rangle$, is distributed in the flow; here u and v are velocity fluctuations in the streamwise coordinate x and the wall-normal coordinate y, respectively, and $\langle \cdot \rangle$ denotes a suitable average. Its behavior in pipe and channel flows is shown qualitatively in Fig. 1. The quantity $\tau^+ \equiv \tau/U_*^2$ increases from its zero value at the wall, apparently like y^3 for small y, and rapidly reaches about half the maximum value at a y^+ of about 12. It continues to increase further to reach a maximum value at y_p. The maximum value equals τ_w in the limit $R_* \to \infty$, but falls short of τ_w at any finite R_*, by an amount, say, $\Delta(R_*)$. The Reynolds stress τ decreases beyond y_p, and reaches zero in the freestream of the boundary layer, and on the centerline of the pipe or channel.

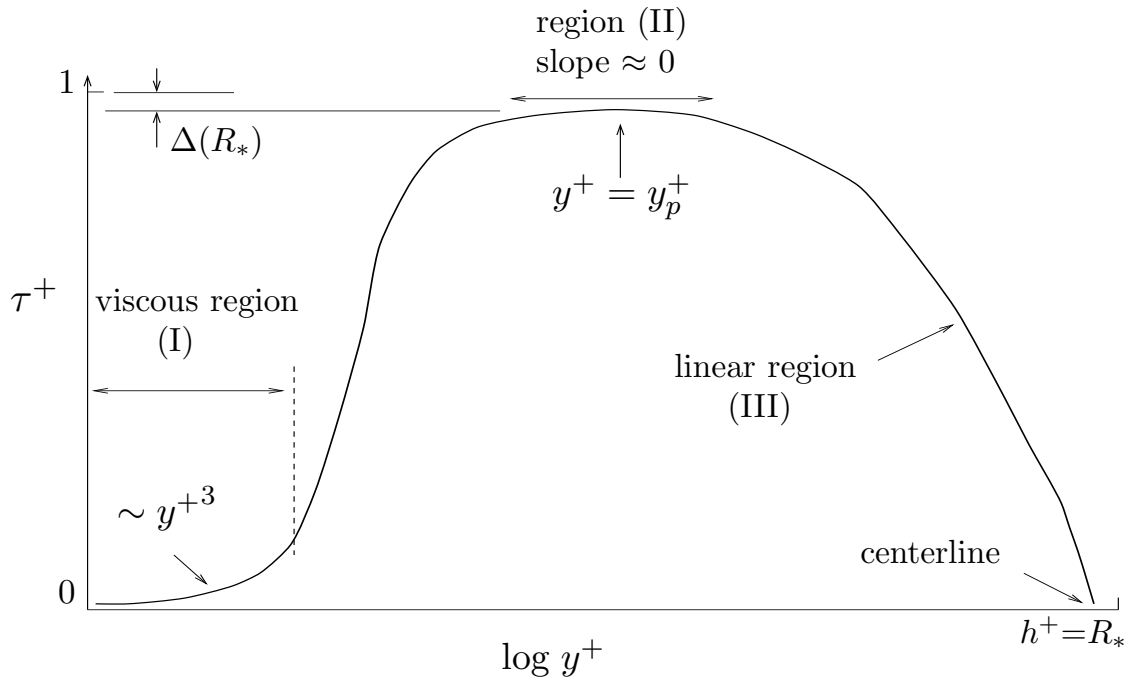

Figure 1: A schematic of the turbulent shear stress τ^+ profile in channel and pipe flows, showing three distinct regions. The buffer layer is interposed between regions I and II.

Of special importance is the position y_p^+. Its leading order variation has been obtained empirically by Long & Chen (1981) and Sreenivasan (1987), who have shown that

$$y_p^+ = \lambda R_*^{1/2}, \tag{4}$$

where $\lambda = 1.87$ and 2, respectively. Although the two prefactors are somewhat different, they agree on the principal result that *the peak of the Reynolds shear stress occurs at a* y^+ *that increases as* $R_*^{1/2}$. We revisit this issue here. Figure 2a shows plots of τ^+ *vs* $y^+/R_*^{1/2}$ for a range of Reynolds numbers. The $R_*^{1/2}$ variation of y_p^+ appears to be a good leading order approximation. There is some correction to this scaling at the lowest R_*, which we shall examine subsequently. For the present, we have ignored the low R_* data in estimating λ. On the basis of Fig. 2a, we take $R_* \leq 500$ as an operational definition of the low Reynolds number. Figure 2b is an expanded plot near the peak of τ^+. An accurate determination of y_p^+ for large R_* is difficult because the peak is rather flat (and becomes more so with increasing R_*) and because there is much scatter in the data. Mindful of these uncertainties we estimate that $\lambda = 1.8 \pm 0.2$.

The point to emphasize is that, for all but the very low R_*, $y_p^+ = O(R_*^{1/2})$ lies well within the classical logarithmic region ($30 \leq y^+ \leq 0.15R_*$). We shall now discuss its role in determining the distribution of the mean velocity in boundary layer flows. The discussion is specialized for analytical convenience to plane channel flow and axisymmetric pipe flow. The simplicity to be gained is that all the terms in the mean momentum equation are independent of the streamwise direction.

2.2 The basic physical idea

The exact mean momentum equation is given by

$$-\frac{\mathrm{d}P}{\mathrm{d}x} + \frac{\mathrm{d}\tau}{\mathrm{d}y} + \nu\frac{\mathrm{d}^2U}{\mathrm{d}y^2} = 0, \tag{5}$$

where P is the mean pressure and U is the mean velocity depending only on y. The Reynolds shear stress term appears in the equation as an unknown. We now make the obvious point that, at the position at which the turbulent shear stress τ is a maximum, i.e., at y_p, the pressure gradient terms are balanced only by viscous terms; the Reynolds stress terms are entirely absent because *the quantity that appears in the momentum equation is the Reynolds shear stress gradient, not the Reynolds shear stress itself.* We have already seen that y_p resides in the part of the boundary layer traditionally thought to be independent of viscosity, or purely inertial. This means that, *within a region in pipes and channels that has been thought to be inertial, there exists a neighborhood within which only viscous terms are capable of balancing the pressure gradient terms nearly entirely.*

How large is this neighborhood? To answer this question, we plot in Fig. 3 the ratio of the Reynolds shear stress gradient term to the viscous term in the vicinity of y_p^+. Using experimental data for the purpose would have generated much scatter, so our estimates are

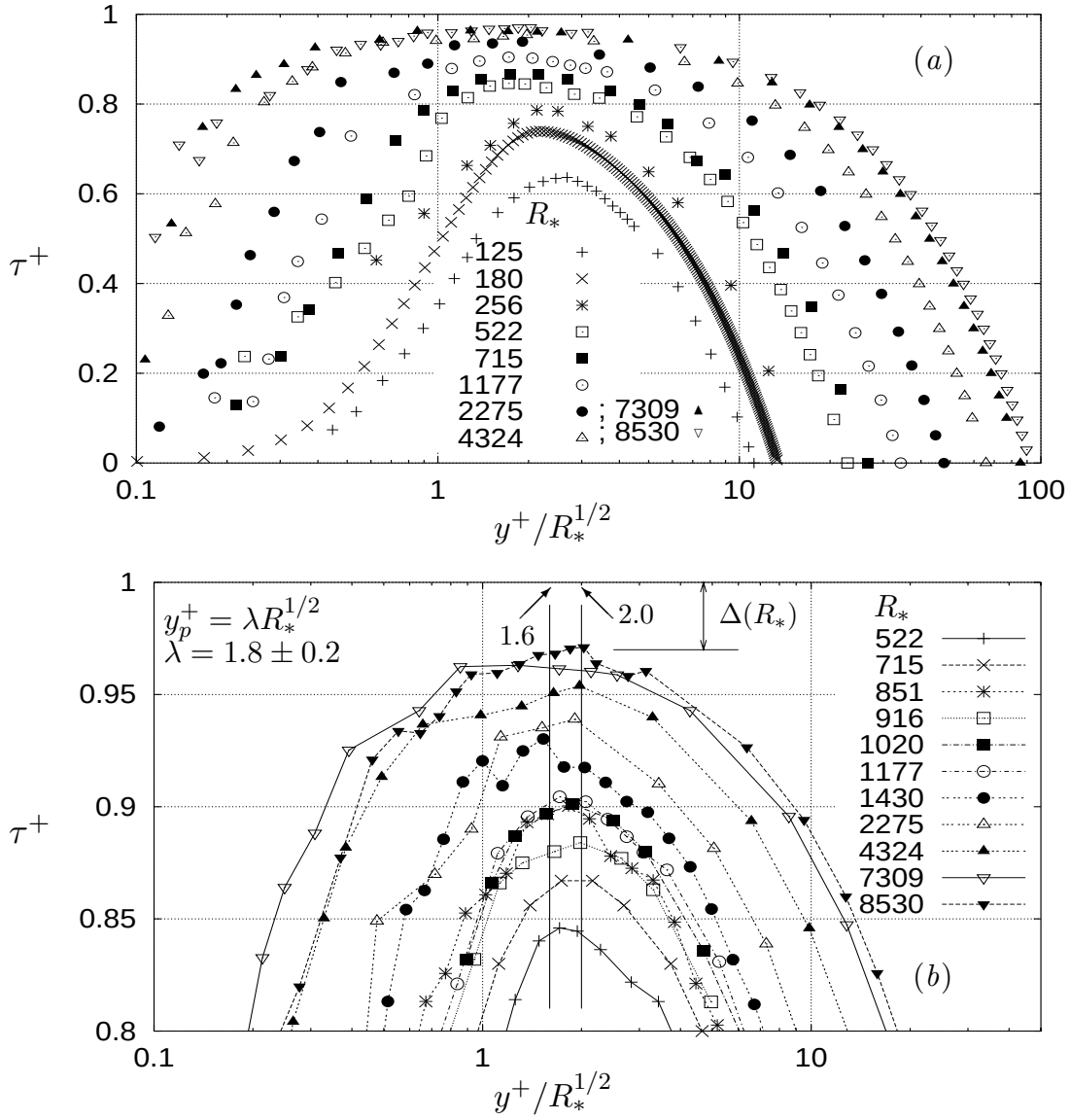

Figure 2: Plots of the turbulent shear stress τ^+ as a function of $y^+/R_*^{1/2}$ (a) across the channel and (b) near its peak for high Reynolds number experiments. The sources for the experimental data are Antonia *et al.* 1992 (channel, $R_* = 256$, 916), Comte-Bellot 1963 (channel, $R_* = 4324$, 7309), Kim *et al.* 1987 (channel DNS, $R_* = 180$), Laufer 1950 (channel, $R_* = 522$, 1177, 2275), Laufer 1954 (pipe, $R_* = 8530$), Sirovich *et al.* 1991 (channel DNS, $R_* = 125$), Wei & Willmarth 1989 (channel, $R_* = 715$, 1020), and Zagarola 1996 (pipe, $R_* = 851$, 1430). The shear stress has been obtained by the numerical differentiation of the measured velocity profile using Eq. (6) of section 3. Zagarola's data for higher Reynolds numbers could not be used because the mean velocity data have not been measured close enough to the wall.

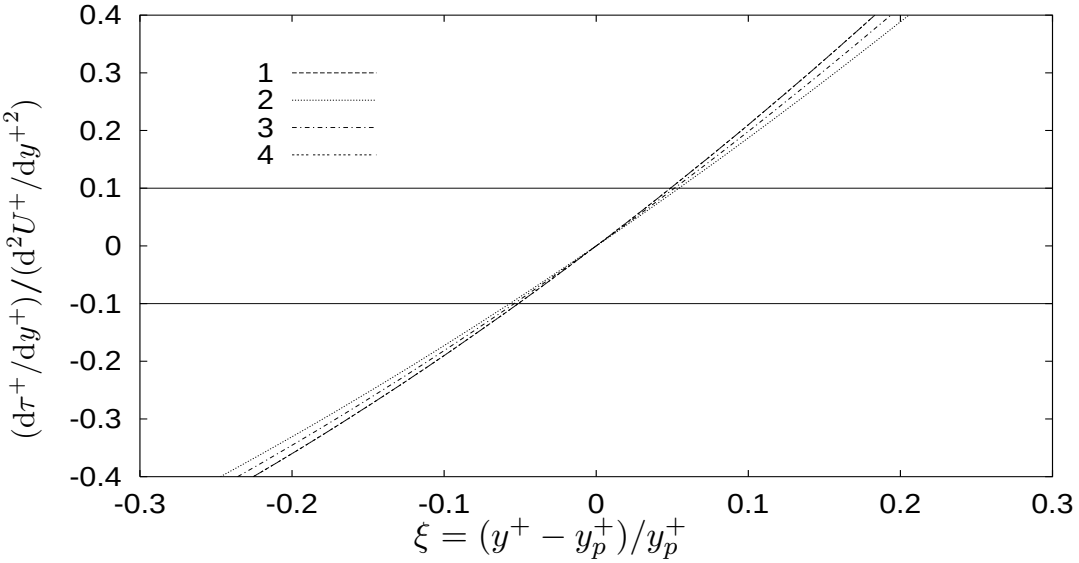

1) $2\xi + \xi^2$ Universal logarithm law

2) $(1+\xi)^{1.8} - 1$
3) $(1+\xi)^{1.9} - 1$
4) $(1+\xi)^{1.95} - 1$
} Barenblatt profile

Figure 3: The ratio of the Reynolds shear stress gradient to the viscous stress gradient in region II around y_p. The four curves are obtained for different fits to the mean velocity data, as explained at the bottom of the figure. The ratio for the Barenblatt profile is given by $(1+\xi)^\alpha - 1$ where $\alpha = 3/(2\ln Re)$.

based on various fits to the data: the classical logarithmic profile and various power-law profiles recommended by Barenblatt (1993). These estimates suggest that the turbulent stress gradient term is of the order of a tenth of the viscous stress gradient term within the region $-0.1 \le \xi \le 0.1$, where $\xi = (y^+ - y_p^+)/y_p^+$. In an order of magnitude sense, the region around y_p^+ where viscous terms overwhelm turbulence terms has itself a width $O(R_*^{1/2})$.

3 The momentum equation

Integrating Eq. (5) and applying the boundary condition at $y = 0$ to obtain the constant of integration, and that at h to eliminate the pressure gradient term, one obtains

$$\frac{\mathrm{d}U^+}{\mathrm{d}y^+} + \tau^+ = 1 - \frac{y^+}{R_*}. \tag{6}$$

It appears natural that we should use Eq. (6) to understand the mean velocity distribution by approximating τ^+ in the form of a double expansion around y_p^+ and about the supremum value of unity (attained in the infinite Reynolds number limit). We have accordingly performed a local analysis (local in y^+), in the limit $R_* \to \infty$, of Eq. (6) in regions I and II and III shown in the typical τ^+ profile of Fig. 1. The regions are defined as domains of validity of the asymptotic expansion of dU^+/dy^+ to the leading order in the following limits:

$$\begin{aligned} R_* \to \infty,\ y^+ = O(1) \qquad & \text{(region I)}, \\ R_* \to \infty,\ y^+ = O(y_p^+) \qquad & \text{(region II)}, \\ R_* \to \infty,\ y^+ = O(R_*) \qquad & \text{(region III)}. \end{aligned}$$

I is the classical viscous region, and III can be thought to be the classical outer region. Viscous terms are significant in both I and II, but the classical buffer region, in which these terms are small in relative magnitude, is interposed between the two regions. This makes the two regions distinct. Here we shall focus on II nearly entirely. The analysis of regions I and III in the same spirit yields some significantly new results (Sahay & Sreenivasan 1996) which will be summarized only as needed.

3.1 Analysis of region II

We can write the Taylor series expansion of τ^+ about y_p^+ as

$$\tau^+(y^+) = \tau^+_{max} + \sum_{n=2}^{\infty} f_n(R_*)\xi^n$$

where $\xi = (y^+ - y_p^+)/y_p^+$, $n! f_n / y_p^{+n} = [\mathrm{d}^n\tau^+/\mathrm{d}^n y^+](y^+ = y_p^+)$, $f_n = o(R_*^\gamma)$ where γ is any positive number, and τ^+_{max} is the maximum value of τ^+ for any given R_*. Clearly, $\tau^+_{max} \leq 1$, the equality holding only at infinite Reynolds number. For any finite Reynolds number, we write $\tau^+_{max} = 1 - \Delta(R_*)$ (see Figs. 1 and 2), where $\Delta = o(1)$. We may thus rewrite the above equation as

$$\tau^+(y^+) = [1 - \Delta(R_*)] + \sum_{n=2}^{\infty} f_n(R_*)\xi^n. \tag{7}$$

Putting (7) into (6) we get

$$\frac{\mathrm{d}U^+}{\mathrm{d}y^+} = \Delta(R_*) - \frac{y_p^+}{R_*} - \frac{y_p^+}{R_*}\xi + \sum_{n=2}^{\infty} f_n(R_*)\xi^n. \tag{8}$$

If we take $\mathrm{d}U^+/\mathrm{d}y^+$ to be positive and monotonic with respect to y^+ (which certainly seems to be case empirically, although a theoretical proof is lacking), we may argue that $\Delta = O(y_p^+/R_*)$: positivity implies $\Delta R_*/y_p^+ = o(R_*^\gamma)$ for any positive γ and monotonicity implies $y_p^+/\Delta R_* = o(R_*^\gamma)$.

The result that $\Delta = O(y_p^+/R_*)$, when used in conjunction with the estimate of y_p^+ (Eq. (4)), yields $\Delta = O(R_*^{-1/2})$, say $aR_*^{-1/2}$, where a is a constant. (This latter relation is verified independently also by experiment.) Using these estimates of the leading order of y_p^+ and Δ we get, from Eq. (8),

$$\frac{\mathrm{d}U^+}{\mathrm{d}y^+} = \frac{a}{R_*^{1/2}} - \frac{\lambda}{R_*^{1/2}} - \frac{\lambda}{R_*^{1/2}}\xi + o(R_*^{-1/2})[1+\xi] + \sum_{n=2}^{\infty} f_n(R_*)\xi^n. \tag{9}$$

Making use of the relation $y^+ = y_p^+(1+\xi) = \lambda R_*^{1/2}(1+\xi)$ we can rearrange (9) to obtain

$$\frac{\mathrm{d}U^+}{\mathrm{d}y^+} = \frac{(a-\lambda)\lambda}{y^+} + \frac{(a-2\lambda)\lambda}{y^+}\xi + o(R_*^{-1/2})[1+\xi] + \sum_{n=2}^{\infty} f_n(R_*)\xi^n. \tag{10}$$

3.2 The logarithmic 'law'

An exact logarithmic profile would obtain if, in a nonzero neighborhood of $\xi = 0$, the first term in Eq. (10) is dominant in the limit $R_* \to \infty, y^+ = O(y_p^+)$. The second term is of the order of the first term and thus can be neglected only if it is identically zero, which requires the exact equality of a and 2λ. This assessment requires a numerical estimate of the constant a, which we examine in Fig. 4.

Here again it is difficult to determine the coefficient accurately owing to finite-Reynolds-number corrections. Ideally, one would consider data in intervals like $[R_*, \infty)$ for increasing R_* and look for convergence of the least-square estimates of the coefficient a. The inset in Fig. 4 shows our attempt at implementing this algorithm within the constraints of finite maximum R_* and small number of data points. Least-square estimates of a are obtained using n data points at the largest available Reynolds numbers. We have taken into account only the data for $R_* \geq 500$. We do not consider smaller than five points (i.e., we stop at $n = 5$) since the fit for a smaller value of n will lead to unacceptable statistical uncertainties. The resulting estimate for a is 3.1 ± 0.1 (see inset).

The uncertainty in the numerical estimates of a and λ allow for the possibility that $a - 2\lambda \equiv 0$, although the use of their mean values makes the second term nonzero. It is clear that empirical estimates will not settle the issue of *exact* equality of the two numbers. An added ignorance factor is the lack of knowledge of the asymptotic behavior of the functions $f_n(R_*)$. For the logarithmic law to exist, the f_n (derivatives of τ^+ at y_p) must be $o(\Delta)$.

In spite of the ambiguity regarding the existence of an *exact* logarithm law in region II, it is true that there exists a nonzero neighborhood around y_p^+ in which a logarithmic variation is a *good approximation* to the true velocity profile. In the extended limit $R_* \to \infty, y^+ = O(y_p^+), \xi \to 0$, the leading term representation of (10) is

$$\frac{\mathrm{d}U^+}{\mathrm{d}y^+} = \frac{(a-\lambda)\lambda}{y^+}, \tag{11}$$

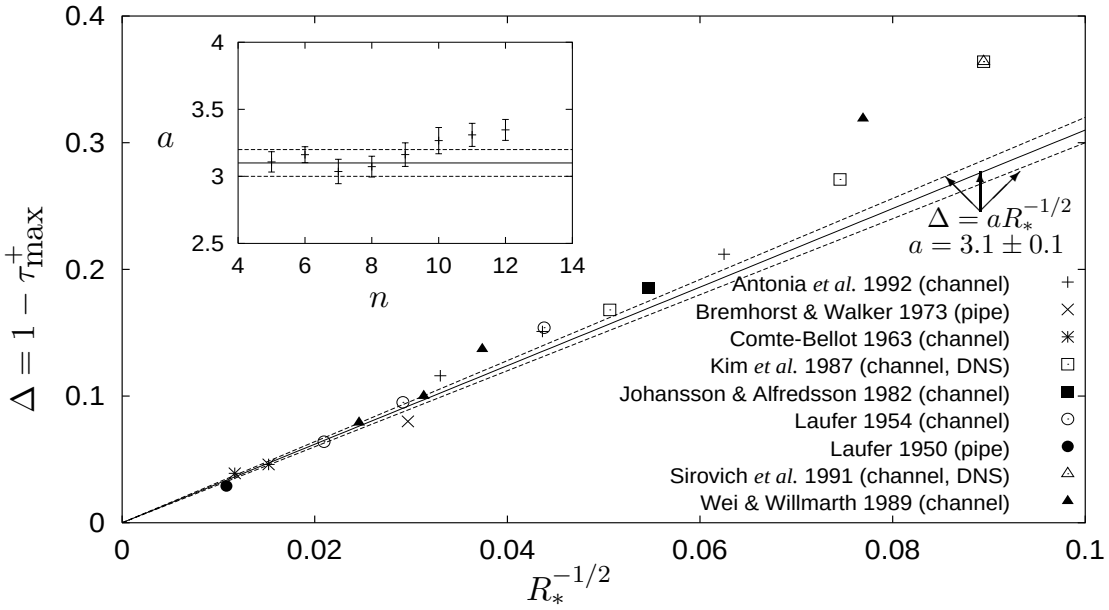

Figure 4: Reynolds number variation of the leading order correction to the peak value of τ^+. The convergence of the estimate of a was checked by varying the number of data-points (n points corresponding to the largest R_*) used for the least-square fit. The variation of a with n is shown in the inset plot. The error bars represent 68% confidence intervals.

just as required for a logarithmic behavior. The log-law constant $1/\kappa$ will then be 2.34 ± 0.8. Despite the large uncertainty, the mean is very close to the traditionally accepted value. A detailed analysis of region III of Fig. 1 (Sahay & Sreenivasan 1996) shows, however, that the outer edge of this logarithmic region is $o(1)$.

3.3 Local structure of the power-law profile

The expression for the profile is (Barenblatt 1993, Barenblatt & Chorin 1996)

$$U^+ = \beta y^{+^\alpha}, \qquad \beta = \frac{1}{\sqrt{3}} \ln Re + \frac{5}{2}, \quad \alpha = \frac{3}{2 \ln Re}, \tag{12}$$

where Re is the Reynolds number based on the pipe diameter and the average velocity across the pipe cross-section. The factor $\sqrt{3}$ in β is an aesthetic choice of the originator of the equation. The basis for the choice of $\ln Re$ in α is that $\ln Re$ is insensitive to the precise definition of Re (see, e.g., Barenblatt & Goldenfeld 1995). The relationship between Re and R_* is implicit in (12) and has been shown to be (Barenblatt 1993)

$$R_* = \frac{1}{2} \left[\frac{e^{3/2\alpha} 2^\alpha \alpha (1+\alpha)(2+\alpha)}{\sqrt{3} + 5\alpha} \right]^{1/(1+\alpha)} . \tag{13}$$

Consider the limit process $R_* \to \infty, y^+ = O(y_a^+)$ where y_a^+ is arbitrary. Let $\zeta = (y^+ - y_a^+)/y_a^+$. We can write Eq. (12) as

$$U^+ = \beta \, \mathrm{e}^{\alpha \ln y_a^+} \, \mathrm{e}^{\alpha \ln(1+\zeta)}. \tag{14}$$

Since ζ is $O(1)$ and α is $O((\ln Re)^{-1})$ the second exponential can be expanded to yield, after some rearrangement,

$$U^+ = (\alpha\beta {y_a^+}^{\alpha}) \ln y^+ + \beta {y_a^+}^{\alpha}(1 - \ln {y_a^+}^{\alpha}) + O((\alpha \ln(1+\zeta))^2). \tag{15}$$

Thus in a small neighborhood around y_a^+ the mean velocity is like a logarithm. The asymptotic forms of the slope ($A \equiv \alpha\beta {y_a^+}^{\alpha}$) and the constant ($C \equiv \beta {y_a^+}^{\alpha}(1 - \ln {y_a^+}^{\alpha})$) will depend upon the order and magnitude of y_a^+. If we take $y_a^+ = aR_*^{\gamma}$ then it follows that

$$A = \mathrm{e}^{3\gamma/2} \left[\frac{\sqrt{3}}{2} + O(\frac{\ln^2 R_*}{\ln R_*}) \right] \tag{16}$$

$$C = \mathrm{e}^{3\gamma/2} \left[\frac{1}{\sqrt{3}} \left(1 - \frac{3\gamma}{2} \right) \ln R_* + O(\ln^2 R_*) \right] \tag{17}$$

where $\ln^2 R_* = \ln(\ln R_*)$. Putting $\gamma = 1$ the logarithmic variation predicted for region III (Barenblatt & Chorin 1996) is obtained. The slope of this logarithmic law is indeed $\sqrt{e}$ times larger than the *universal* log-law.

It is of interest to examine the local structure of Eq. (12) near y_p^+. The local logarithmic approximation (15) will hold with y_a^+ replaced by y_p^+. To calculate the asymptotic forms of the slope and the constant (labeled A_p and C_p respectively) we need an expression for $y_p^+(R_*)$ which is consistent with the power-law expression for U^+, Eq. (12). This can be done by substituting (12) in the mean momentum equation (6) and solving for $y^+ = y_p^+$ at which $\mathrm{d}\tau^+/\mathrm{d}y^+ = 0$. These manipulations yield

$$y_p^+ = \left((1-\alpha)\alpha\beta R_* \right)^{1/(2-\alpha)}. \tag{18}$$

In the limit $R_* \to \infty$, Eq. (18) can be written as

$$y_p^+ = R_*^{1/2} \mathrm{e}^{3/8} \left(\frac{\sqrt{3}}{2} \right)^{1/2} \left[1 + \sum_{n=1}^{\infty} \sum_{m=0}^{n} P_{mn} \frac{(\ln^2 R_*)^m}{(\ln R_*)^n} \right] \tag{19}$$

where P_{mn} are constants. The asymptotic forms of A_p and C_p can easily be obtained.

The form of U^+ at y_p^+ corresponding to the power-law (12) can be derived in a rational way from the mean momentum equation, along the lines of the analysis in section 3.1. We take into account (possible) corrections to the leading order of y_p^+ and assume

$$y_p^+ = \lambda R_*^{1/2} \left[1 + \sum_{n=1}^{\infty} \sum_{m=0}^{n} \lambda_{mn} \frac{(\ln^2 R_*)^m}{(\ln R_*)^n} \right] \tag{20}$$

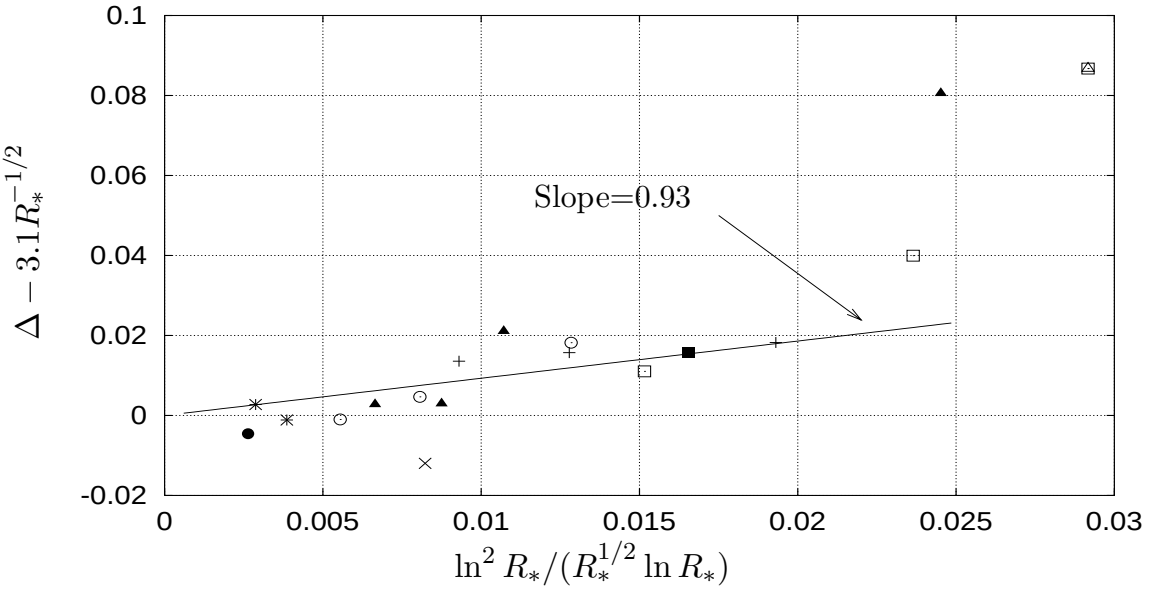

Figure 5: The difference between Δ and the leading order behavior $3.1R_*^{-1/2}$, plotted against $\ln^2 R_*/(R_*^{1/2} \ln R_*)$, in order to determine the next-order term in Eq. (21). Using the best fit to the data (except for those at the lowest three Reynolds numbers) yields the relation $\Delta = 3.1R_*^{-1/2}(1 + 0.3 \ln^2 R_*/\ln R_*)$. The symbols key is identical to that of Fig. 4.

in accordance with (19). It is prudent to resolve Δ to the same degree as y_p^+, hence we take

$$\Delta = aR_*^{-1/2}\left[1 + \sum_{n=1}^{\infty}\sum_{m=0}^{n} a_{mn}\frac{(\ln^2 R_*)^m}{(\ln R_*)^n}\right]. \tag{21}$$

The logarithmic 'correction terms' to the leading order dependence of Δ on R_* are not unrealistic. For example, returning to Fig. 4, it is seen that the $R_*^{-1/2}$ dependence is good only at very large R_*. In Fig. 5, we show the difference $\Delta - aR_*^{-1/2}$, which itself behaves to the leading order as $\ln^2 R_*/(R_*^{1/2} \ln R_*)$, just as supposed in the expansion (21).

Using Eqs. (20), (21) and the relation $y^+ = y_p^+(1 + \zeta)$, we obtain an expression similar to (10) for the velocity derivate

$$\begin{aligned}\frac{\mathrm{d}U^+}{\mathrm{d}y^+} = {} & \frac{a\lambda}{y^+}(1+\zeta)\left[1 + \sum_{n=1}^{\infty}\sum_{m=0}^{n} a'_{mn}\frac{(\ln^2 R_*)^m}{(\ln R_*)^n}\right] \\ & - \frac{\lambda^2(1+\zeta)^2}{y^+}\left[1 + \sum_{n=1}^{\infty}\sum_{m=0}^{n} \lambda'_{mn}\frac{(\ln^2 R_*)^m}{(\ln R_*)^n}\right] + \sum_{n=2}^{\infty} f_n\zeta^n \end{aligned} \tag{22}$$

where a'_{mn} and λ'_{mn} are constants related to a_{mn} and λ_{mn}. In the extended limit $R_* \to \infty, y^+ = O(y_p^+), \zeta \to 0$ the leading term of (22) is of the same form as that of $\mathrm{d}U^+/\mathrm{d}y^+$ for the Barenblatt profile.

In summary, it appears that the Barenblatt–Chorin profile is consistent with Eq. (6) when the double series expansions (20) and (21) are used for y_p^+ and Δ.

4 Conclusions

The primary qualitative point of this work is that there exists a mechanism for viscous effects to spread to the classical overlap region. The existence of such a mechanism will in principle prevent classical matching, so that the leading order 'inner' and 'outer' expansions are technically insufficient to construct a uniformly valid approximation of the mean velocity profile.

What, then, can be said about the classical log-law? First, it must be noted that the velocity change across the 'mesolayer' is not of the order unity, unlike in most boundary layer problems, which may make its importance potentially less significant. Second, just as is done here for region II, we have analyzed regions I and III in some detail, making use of the well-known forms of the Reynolds shear stress distributions in those regions. (For example, in region III, one has a linear distribution of the Reynolds shear stress, with some well-understood finite Reynolds number corrections.) It is then possible to patch together the results from all three regions. A summary of this work is as follows. In region I, beyond about $y^+ \sim 30$, dU^+/dy^+ lies close to that implied by the classical logarithmic law. In region II, we have already seen that the log-law can be a good approximation (and even exact in a small neighborhood of y_p^+). In region III, dU^+/dy^+ lies close to the classical value for y^+ smaller than $0.15R_*$. It is therefore reasonable that one can smoothly match the three regions and obtain a logarithmic variation of velocity between $y^+ \sim 30$ and $y^+ \sim 0.15R_*$, regardless of whether it is exact.

What can be said of power-laws, in particular the Barenblatt profile? In our present view, a self-consistent way of understanding the origin of this profile is to use Eq. (6) and the appropriate expansions for Δ and y_p in B1 (and the appropriate version of y_a in region B2). We believe that the rich structure of power-law profiles makes them fit the data well. However, a close analysis of region III (Sahay & Sreenivasan 1996) reveals that asymptotically the velocity profile cannot be exactly logarithmic in B2. The most significant point in favor of power laws is that they account, in some fashion, for viscous effects to pervade in the classical overlap region.

The importance of viscous effects in a region traditionally thought to be inviscid has other obvious analogies. The principal analogy is the Kolmogorov spectral cascade. Just as viscous effects are centered around the peak position of the Reynolds shear stress in the present problem, one may imagine the viscous effects in Kolmogorov turbulence may be centered around the position of maximum energy transfer in wave number space. This provides a natural mechanism for viscous effects to encroach the inertial region of the spectral space. Details are currently being worked out.

We have so far not speculated on the physical origin of the viscous effects in the neighborhood of y_p. Two possible scenarios present themselves. It may well be that the bursting

of wall-layer streaks (which undoubtedly extend beyond the sublayer) carry viscous effects with them as they penetrate up to $y^+ = O(R_*^{1/2})$. Alternatively, the viscous cores of the coherent vortices in the 'critical layer' region are such that their effects do not vanish at any Reynolds number (Barenblatt 1993). Whatever the mechanism, it appears (Sreenivasan 1987) that the 'critical layer' or the mesolayer plays an important role in the dynamics of wall flows that cannot be subsumed in the classical picture.

Acknowledgements

The work was supported by a grant from AFOSR.

References

Antonia, R. A., Teitel, M., Kim, J. & Browne, L. B. 1992 Low Reynolds-number effects in a fully developed turbulent channel flow. *J. Fluid Mech.* **236**, 579–605.

Barenblatt, G. I. 1993 Scaling laws for fully developed turbulent shear flows. Part 1. Basic hypotheses and analysis. *J. Fluid Mech.* **248**, 513–520.

Barenblatt, G. I. & Chorin, A. J. 1996 Scaling laws and zero viscosity limits for wall-bounded shear flows and for local structure in developed turbulence. *Proc. Nat. Acad. Sci.* **93**, 6749–6752.

Barenblatt, G. I. & Goldenfeld, N. 1995 Does fully developed turbulence exist? Reynolds number independence versus asymptotic covariance. *Phys. Fluids* **7**, 3078–82.

Bremhorst, K. & Walker, T. B. 1973 Spectral measurements of turbulent momentum transfer in fully developed pipe flow. *J. Fluid Mech.* **61**, 173–186.

Coles, D. E. & Hirst, E. A. 1969 *Proc. Computation of Turbulent Boundary Layers—1968 AFOSR–IFP–Stanford Conference, Vol II.*

Comte-Bellot, G. 1963 *Contribution a l'étude de la turbulence de conduite.* Ph.D. thesis, University of Grenoble. Trans. Bradshaw, P. 1969 *Turbulent Flow Between Two Parallel Walls*, ARC31609, FM 4102.

Domb, C. & Green, M. S., eds. 1976 *Phase Transitions and Critical Phenomena.* NY: Academic Press.

Drazin, P. G. & Reid, W. H. 1981 *Hydrodynamic Stability.* Cambridge: Cambridge University Press.

Dussauge, J. P., Smith, R. W., Smits, A. J., Fernholz, H., Finley, P. J. & Spina, E. F. 1996 *Turbulent Boundary Layers in Subsonic and Supersonic Flow.* AGARDograph 335, NATO, France.

George, W. K. & Castillo, L. 1996 A theory for turbulent pipe and channel flows. Preprint.

George, W. K., Castillo, L. & Knecht, P. 1996 The zero pressure-gradient turbulent boundary layer, Turbulence Research laboratory Tech. Rep. TRL-153, School of Engineering and Applied Sciences, SUNY Buffalo, NY.

Head, M. R. & Bandyopadhyay, P. R. 1981 New aspects of turbulent boundary-layer structure. *J. Fluid Mech.* **107**, 297–338.

Johansson, A. V. & Alfredsson, P. H. 1982 On the structure of turbulent channel flow. *J. Fluid Mech.* **122**, 295–314.

Kim, J., Moin, P. & Moser, R. 1987 Turbulence statistics in fully developed channel flow at low Reynolds number. *J. Fluid Mech.* **177**, 133–166.

Kline, S. J., Reynolds, W. C., Schraub, F. A. & Runstadler, P. W. 1967 The structure of turbulent boundary layers. *J. Fluid Mech.* **30**(4), 741–773.

Laufer, J. 1950 Investigation of turbulent flow in a two-dimensional channel. Technical Report NACA-1053.

Laufer, J. 1954 The structure of turbulence in fully developed pipe flow. Technical Report NACA-1174.

Long, R. R. & Chen, T.-C. 1981 Experimental evidence for the existence of the 'mesolayer' in turbulent systems. *J. Fluid Mech.* **105**, 19–59.

Monin, A. S. & Yaglom, A. M. 1971 *Statistical Fluid Mechanics: Mechanics of Turbulence, vol. I.* Cambridge: MIT press.

Monin, A. S. & Yaglom, A. M. 1975 *Statistical Fluid Mechanics: Mechanics of Turbulence, vol. II.* Cambridge: MIT press.

Rao, K. N., Narasimha, R. & Badri Narayanan, M. A. 1971 The bursting phenomenon in a turbulent boundary layer. *J. Fluid Mech.* **48**, 339–352.

Sahay, A. & Sreenivasan, K. R. 1996 The structure of the mean velocity profile in turbulent channel and pipe flows. Preprint.

Sirovich, L., Ball, K. S. & Handler, R. A. 1991 Propagating structures in wall-bounded turbulent flows. *Theor. Comput. Fluid. Dyn.* **2**, 307–317.

Sreenivasan, K. R. 1987 A unified view of the origin and morphology of the turbulent boundary layer structure. In *Turbulence Management and Relaminarisation* (eds. H. W. Liepmann & R. Narasimha), pp. 37–61. Springer-Verlag.

Sreenivasan, K. R. 1989 The turbulent boundary layer. In *Frontiers in Experimental Fluid Mechanics* (ed. Gad-el-Hak), pp. 159–209. Berlin: Springer-Verlag.

Tennekes, H. & Lumley, J. L. 1972 *A First Course in Turbulence.* Cambridge, MA: MIT Press.

Wei, T. & Willmarth, W. W. 1989 Reynolds number effects on the structure of a turbulent channel flow. *J. Fluid Mech.* **204**, 57–95.

Zagarola, M. V. 1996. *Mean Flow Scaling of Turbulent Pipe Flow.* Ph.D. thesis, Department of Mechanical and Aerospace Engineering, Princeton University.

Zagarola, M. V. & Smits, A. J. 1997 Scaling of the mean velocity profile for turbulent pipe flow. *Phy. Rev. Lett.* **78** (in press).